Passive and active flow control using vortex methods

Georges-Henri Cottet, Roland Hildebrand, Petros Koumoutsakos, Chloé Mimeau, Iraj Mortazavi, Philippe Poncet

Proceedings of the 6th International Conference on
Vortex Flows and Vortex Models (ICVFM Nagoya 2014)
November 17 - 20, 2014, Nagoya, Japan

Passive and active flow control using vortex methods

Geoges-HenriCottet[1)], Roland Hildebrand[1)], Petros Koumoutsakos[2)], Chloe Mimeau[1,3)], Iraj Mortazavi [2)] and Philippe Poncet[4)]

[1)]Laboratoire Jean Kuntzmann, CNRS and University Grenoble-Alpes, Grenoble, France
[2)]Computational Science, ETH Zurich, Zurich, Switzerland
[3)]Institut de Mathématiques de Bordeaux, CNRS, INRIA and University of Bordeaux, Bordeaux, France
[4)]Lab. Mathematics and their Applications, CNRS and Universié de Pau et des Pays de l'Adour, Pau, France

This paper deals with the application of remeshed particle methods for the simulation and control of wakes behind obstacles. We consider passive as well as active control strategies. Active control consists of jets at the boundary and we show how enhancing natural 3D instabilities of the flow can reduce the drag. Passive control strategies consist of porous coatings on the obstacle and we investigate optimal locations of the porous coating to regularize the wake downstream and reduce the drag.

Keywords: Cylinder wakes, Drag reduction, Porous medium, Vortex method, Penalization method

1. Introduction

The control of wakes remains a challenging topic of great importance in aircraft and automobile industry. Depending on the particular application, wake control can have various goals and can be achieved either by passive or active strategies. Active control implies that one is ready to impart energy on the flow by means of actuators on the surface of the obstacle, keeping in mind that this energy must be included in the global energy budget to conclude on the efficiency of the particular control strategy. Most often passive control consists of shape optimization based on the addition of appendices like foilers or ribblets on the surface of the obstacle. Another possibility is to locally modify the physical properties of the body surfaces. In all cases, the goal is to modify the boundary layer, either in order to minimize the production of vorticity, and thus the global strength of the wake, or to produce a wake that is organized in a way that will reduce its impact on the drag value.

In this paper we will review works in our group in the two directions outlined above. In the first part we will focus on active control strategies which consist of jets located on the surface of the body [1]. The body is a circular cylinder. We in particular investigate how to devise efficient 3D strategies and how optimal 3D solutions differ from their 2D counterpart. In this case the topology of the wake, and not only its strength, impacts the drag forces. Active control using three-dimensional parameters turns out to be much more efficient than for the 2D case.

In the second part, we consider 2D passive control devices consisting of porous coatings on the surface of the body [2]. In this case the body is a semicircular cylinder seen a prototype for an outside mirror. We in particular investigate the effect of the size and location of the porous coating both on the enstrophy production and drag values.

In both cases the simulation method is a remeshed particle method for the vorticity formulation of the Navier-Stokes equations, but the methods to enforce boundary conditions at the body differ. In the first case, we use vorticity fluxes [3,4,5] on a cylindrical body-fitted mesh. In the second case we use a penalization method on a cartesian mesh independent of the body geometry [6].

2. Active control of the wake of a cylinder

The 2D and 3D cylinder are classical benchmarks to investigate the physical properties of wakes and the relationship between these properties and the values of the drag. Since the works of [7,8,9,10] it is known that manipulations of the body velocity can have strong impact on the wake topology and thus on the values of the drag.

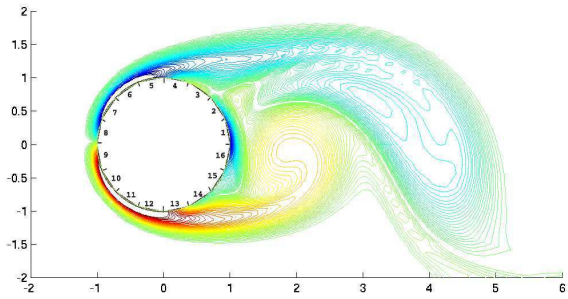

Figure 1: Actuator configuration on the cylinder surface (left, from [11]) and velocity profile fitting the best population obtained by the CGA (right).

2.1. The 2D case

A systematic study has been done in [11] to identify the tangential velocity profiles that would be optimal for drag reduction. In this work the velocity controllers consisted of tangential velocities with a given energy and the optimization technique was a clustering genetic algorithm. The surface of the cylinder was divided into 16 panels as shown on Fig.1. In the optimal configuration, the drag reduction resulted essentially from the action of the actuators 3-4 ad 13-14, at an angle of about $\pi/3$ downstream on the surface of the cylinder, that is close to the separation point.

2.2 The 3D case

Although the geometry of a cylinder is two-dimensional, it spontaneously generates three-dimensional instabilities. Remarkably, these three dimensional instabilities go with a decrease of the drag (see Fig. **??**). It is therefore natural to expect that control devices can be more efficient if they reinforce these three dimensional instabilities. The idea is therefore to start from the two-dimensional profile identified above, and to superimpose a three-dimensional modulation on top of this pro-

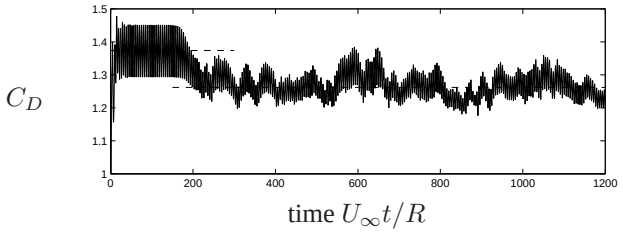

Figure 2: Evolution of the drag coefficient for a three-dimensional cylinder wake at $Re = 300$ (the dashed lines denote the reference values 1.374 and 1.262) showing the drag decay when the flow become 3D. From [11].]

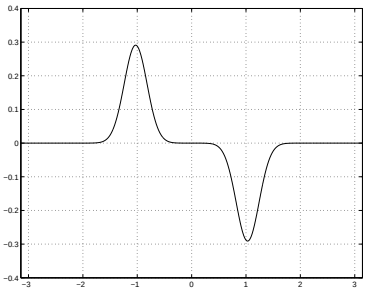

Figure 3: Tangential velocity profile as a function of the angle to miniize 2D drag. From [1].

file.

One first needs to define a continuous profile that matches the discrete values obtained in [11]. The following function fulfills this goal

$$f(\theta) = \alpha \sum_{j=1,2} \frac{(-1)^j}{\sigma\sqrt{2\pi}} \exp\left(\frac{-(x+(-1)^j m)^2}{2\sigma^2}\right) \qquad (1)$$

with $\alpha = 0.3342$, $m = 1.03$ and $\sigma = 0.21$. It is plotted on Fig. **??**.

Simulation method. As we will se the optimization technique relies on repeated 3D simulations. It is therefore necessary to have at hand a numerical method which is both inexpensive and reliable. Remeshed vortex methods were designed in [3] to fulfill these properties for 2D wakes. Extensions for the simulation of 3D wakes work as follows.

- The vorticity field is discretized on particles: $\omega(\boldsymbol{x}, t) = \sum_p \omega_p \delta(\boldsymbol{x} - \boldsymbol{x}_p(t))$
- The particles $\boldsymbol{x}_p$ are convected with the flow velocity:

  $d\boldsymbol{x}_p/dt = \boldsymbol{u}(\boldsymbol{x}_p, t)$

  A second order Runge-Kutta scheme is used to integrate the equations of motion.
- At each time step, particles are remeshed onto a cylindrical grid. On this grid the velocity field is evaluated with no-through flow conditions, using a second order, FFT-based, Poisson solver. The strengths of the particles are modified on the grid to account for vortex stretching and diffusion.

Case	Mode coefficients c_0 or $(a_k^2 + b_k^2)^{1/2}$					C_D
	$k=0$	$k=1$	$k=2$	$k=3$	$k=4$	$Re=300$
I	0	0	0	0	0	1.26
II	0.316	0	0	0	0	1.143
III	0.22	0.139	0.015	0.011	0.178	0.862

Table 1: Averaged drag : no control (Case I), 2D control (Case II), optimal 3D control (Case III). From [1].

- The wall boundary conditions are translated into vorticity fluxes for the tangential components of the vorticity and homogeneous Dirichlet condition for the normal component. (see for instance [12,4,13]).

The Lagrangian treatment of the vorticity advection method allows the use of comparatively small computational domains and large time-steps without compromising neither the stability nor the accuracy of the method in the presence of strong variations in the boundary conditions [4]. In the optimization runs, the cylindrical (r, θ, z) computational domain was extending to $R_{\max} = 1 + 4\pi in the radial direction and L = \pi D$ in the spanwise direction, where D is the cylinder diameter. For $Re = 300$, the resolution was set to $256 \times 128 \times 64$ grid points. For $Re = 1000$, the resolution was doubled in all directions, with a time step $\delta t = 0.0625$.

Optimization strategy and results. The 3D control velocity profiles of the present optimization study are spanwise modulations of the 2D profile given above. The velocity profile is parameterized in terms of harmonics of the cylinder span :

$$U_\theta(\theta, z) = U_\infty\, f(\theta) \left(c_0 + \sqrt{2}\sum_{k=1}^{n} a_k \sin(2\pi k z/L) + b_k \cos(2\pi k z/L)\right) \boldsymbol{e}_\theta$$

where the harmonics have a wavelength $\lambda_k = L/k$. We have selected $n = 4$ resulting in 9 parameters for the optimization. Note that the modes $k = 1$, $k = 3$ correspond to the so-called A and B natural modes of the natural instabilities in the cylinder wake [14]. The coefficients c_0 and a_k, b_k are determined under the constraint of constant energy. To roughly match the energy corresponding to the blowing and suction control of [10] the following condition is imposed

$$c_0^2 + \sum_k |a_k|^2 + |b_k|^2 = 0.1.$$

The opimization method proceeds as follows : systematic search on each plane given by two coefficients is done by running the flow equations for $Re = 300$. Then, around each plane minimum, a local gradient descent is performed to further improve the efficiency of the control. This procedure led to the parameters and drag values indicated on table 1. The drag reduction reaches about 30% for the 3D control, to be compared to about 10% for the 2D control. Fig. 4 is a top view of isosurfaces of the vorticity magnitude. On can see that the 3D control enhances the production of streamwise vorticity and weakens the strength of the Karman rollers.

The same perturbation parameters were used to run a case at a Reynolds number of 1000. In that case also the 3D control proved to be much more efficient than its 2D counterpart (see

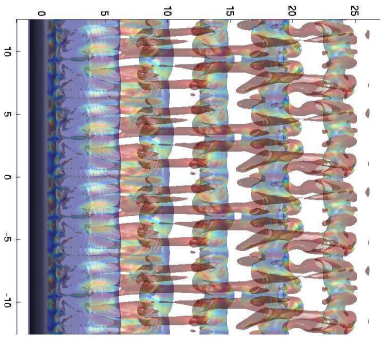

Case I

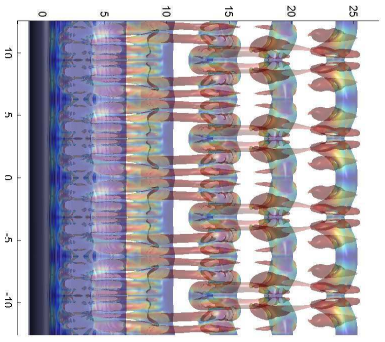

Case II

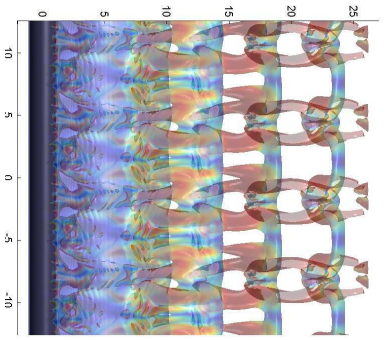

Case III

Figure 4: Top views of isovorticity surfaces for the uncontrolled (Case I), 2D control (Case II) and 3D control (case III) for $Re = 300$. From [1].

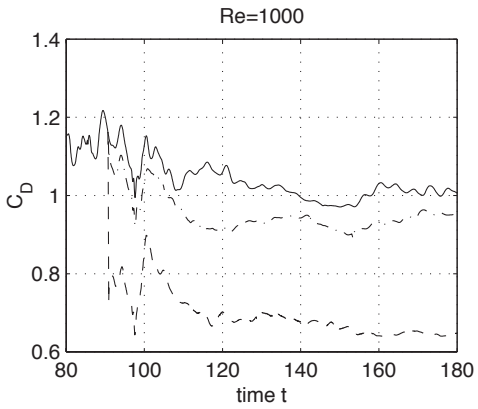

Figure 5: Drag time history for $Re = 1,000$: uncontrolled flow (—, Case I), 2D control ($- \cdot -$, Case II), and optimal 3D control ($--$, Case III). From [1].

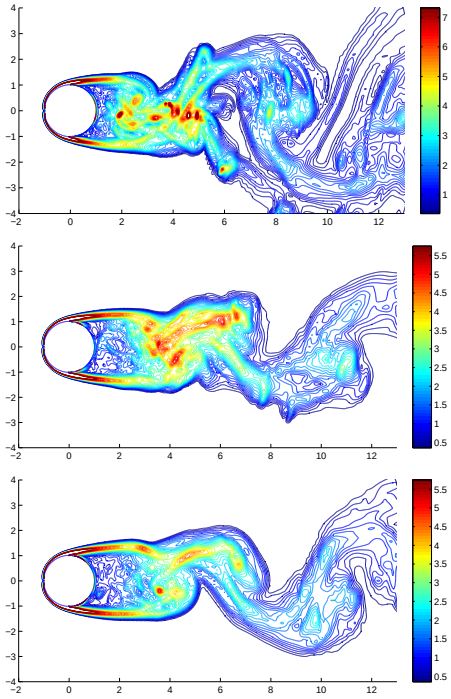

Figure 6: Contours of spanwise quadratic averaged vorticity at $Re = 1000$: without control (top picture), with optimal 2D control (middle picture), and with the parameters of Case III (bottom picture). From [1].

Fig. **??**). The 3D control in that case appears to have also a smoothing effect in the near wake, as shown on Fig. **??**.

3. Passive control by porous coating External mirrors, although they represent only a small portion of the surface of the car (about 0.5%) can be responsible of up to 10% of the total drag. For these devices it would be very difficult to implement active control strategies. Here we investigate passive control strategies that consist of a porous coating laid on the surface of the body.

3.1. Physical setup

The prototype geometry we consider is a semi-cylinder and the porous coating consist of a layer that can be either uniformly laid on the surface, or only at the tips of the surface. We will consider various porosity, thickness and distributions of the porous coating, as shown on Fig. **??**.

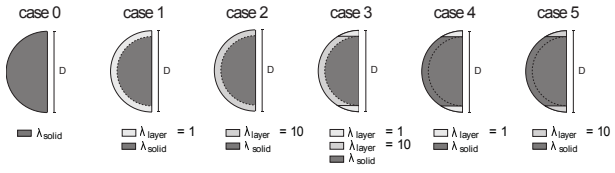

Figure 7: Cases 1 to 5 corresponding to different porous layer configurations. Case 0 depicts the uncontrolled case.

Following [15] the transition between the fluid and the solid can be decomposed in 5 different zones. The first one is the boundary layer inside the porous medium, close to the solid wall. The second region is occupied by and homogeneous

porous flow with Darcy velocity (numbers 1 and 2 in Fig. **??**). In the vicinity of the porous-fluid interface, two transient layers can be recognized (numbers 3 and 4 in Fig. **??**). The first one corresponds to the increase of the porous layer velocity to reach the value $\boldsymbol{u}_i$ at the interface and the second one corresponds to the fluid boundary layer located at at the interface with the free flow. The width of the fluid boundary layer is determined by $\boldsymbol{u}_0 - \boldsymbol{u}_i$ where $\boldsymbol{u}_0$ denotes the velocity of the main fluid flow (number 5 in Fig. **??**).

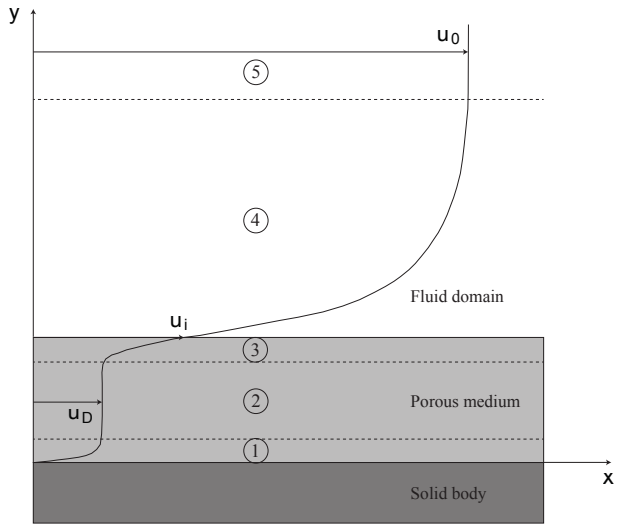

Figure 8: Velocity profile in the vicinity of a porous medium. From [2].

3.1. Simulation method

Like in the previous section the numerical method was a remeshed vorticity particle methods. However the method differs by the way the no-slip condition at the body is handled. In the present case a penalization method was chosen [16]. The idea behind this method is to consider the whole fluid-solid system as a single flow, governed by the Navier-Stokes equation, with a porosity varying from 0 in the fluid to infinity in the solid. This model, originally expressed in velocity-pressure formulation in [16], has been extended to the vorticity formulation [6]. An improved implementation of this method has been proposed in [17].

For the flow around a solid body S he penalization method amounts to solving the following equation

$$\frac{\partial \omega}{\partial t} + (\mathbf{u}.\nabla)\omega = \frac{1}{\mathrm{Re}}\Delta\omega + \nabla \times [\lambda\, \chi_S(\mathbf{u_s} - \mathbf{u})], \tag{2}$$

complemented with inflow and outflow boundary conditions at the boundary of the computational domain. In the above equation χ_S is the characteristic function of S and λ is a large coefficient (inverse of the porosity of the solid). In practice this equation is solved in a time-splitting algorithm, alternating advection, diffusion and penalization steps. For stability reasons the penalizations is solved in an implicit fashion. If Δt denotes the time step, the penalization step to obtain the new vorticity field from the previous velocity field reads

$$\boldsymbol{\omega}^{n+1} = \boldsymbol{\nabla} \times \left[\frac{\boldsymbol{u}^n + \lambda \Delta t \chi_S {\mathbf{u_s}}^n}{1 + \lambda \Delta t \chi_S} \right]. \tag{3}$$

One nice feature of this model is that it allows to use cartesian grids, even for complex geometries, and therefore in particular to use fast Poisson solvers to compute the velocity from the vorticity, and to handle moving objects. It has in particular been used with success to find optimal swimming modes for fishes [18,19].

In the context of the present work, it offers one more advantage. If the obstacle is made of a solid part surrounded by a porous medium, the same flow model can be used to handle all components of the system, by varying the porosity coefficient and thus the parameter λ. This approach can be seen as an alternative to approaches where one solves the porous flow enforcing appropriate porous-fluid boundary conditions [20] or where the Darcy equations are coupled with the Navier-Stokes equations though appropriate interface conditions [21,22].

In all the experiments shown in the following, the semi-circular cylinder has a dimensionless diameter of $d = 1$ including a porous layer of thickness τ, centered at $(x, y) = (0,\ 0)$ in the computational domain $D = [-4,\ 8] \times [-5,\ 5]$. Two values of the Reynolds number are considered : $Re = 550$ and $Re = 3,000$. These two values correspond to laminar flows, which allows to remain in the DNS regime, and allow to investigate the effect of the transition to turbulence.

Results and discussion We first consider the case of a uniform coating (cases 1 to 3) and investigate the effect of the porosity coefficient. In these experiments the width of the porous layer is fixed to 10% of the diameter of the solid body.

Figure **??** shows the evolution of the drag and enstrophy. One can observe that beyond $\lambda = 100$ the porous coating has no effect on the drag. It is interesting to observe that if λ is of the order of 1, which corresponds to a very permeable coating, the drag is roughly equal to its value for the reduce cylinder, but the enstrophy is about 10% below. This shows that the porous coating has a visible regularizing effect.

At this stage, one can conclude that a uniform coating has little or no effect, except for values of the permeability which do not seem realistic from the practical point of view.

The table **??** summarizes the results obtained in all configurations and allows to measure the effect of the location of the porous coating.

	Re $= 550$	
$\tau = 10\%d$	F_x	Enstrophy
case 0 (no control)	0.977	158.4
case 1	0.695 (-29%)	97.5 (-38%)
case 2	0.970 (-0.7%)	114.4 (-28%)
case 3	0.668 (-32%)	87.4 (-45%)
case 4	0.551 (-44%)	110.2 (-30%)
case 5	0.738 (-24%)	125.2 (-21%)

Table 2: Reduction effects resulting from the different porous layer configurations compared to the uncontrolled case at Re=550 with a coating width $\tau = 10\%d$. From [2].

These results show how important the location of the porous coating is. Case 4 strikingly outperforms case 1, although it involves the same permeability coefficient, on a smaller surface. Similarly, case 5 outperforms case 2. The same trends can be seen for the higher Reynolds number case (see Table **??**). In that case a uniform coating with $\lambda = 10$ produces even more

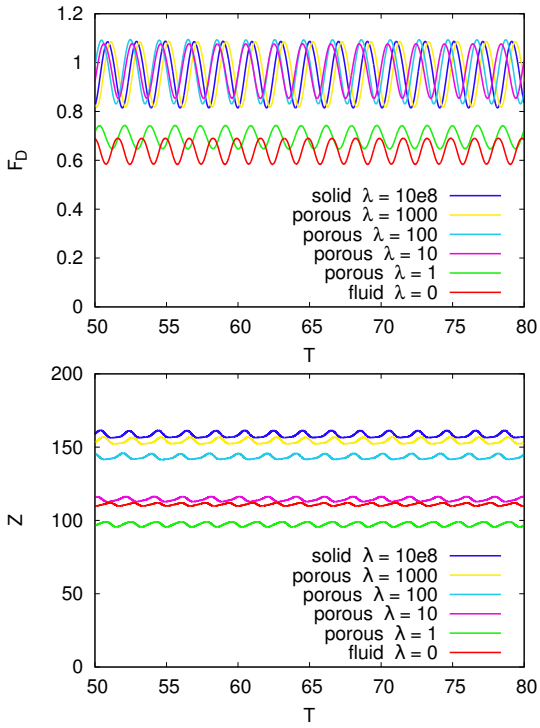

Figure 9: Effects of various layer permeabilities on drag force (left) and enstrophy (right) for the flow past a semi-circular cylinder at Re=550. From [2].

	Re = 3000	
$\tau = 10\%d$	F_x	Enstrophy
case 0 (no control)	0.926	334.2
case 1	0.870 (-6%)	236.7 (-29%)
case 2	1.054 (+14%)	248.8 (-26%)
case 3	0.922 (-0.4%)	223.2 (-33%)
case 4	0.737 (-20%)	270.6 (-19%)
case 5	0.860 (-7%)	281.3 (-16%)

Table 3: Same as Table **??** for $Re = 3000$. From [2].

drag that the uncontrolled configuration. In all cases he layers laid on the tips with $\lambda = 10$ give approximately the same drag reduction than the uniform coatings with $\lambda = 1$. As we will se below, the reason of these performances is that the crosswise width of the wake is smaller when the porous coating is only placed on the tips.

We finally investigate the impact of the porous layer width. Reducing the width of the porous layer makes the performance of the control even more sensitive to its location. We show in Tables **??** and **??** the drags obtained in Cases 1 to 5 for a porous layer width of 2.5% of the diameter. It is remarkable that, for $Re = 3,000$, cases 4 and 5, where the porous layer is only located at the tips, are the only cases which yields drag reduction. It is also interesting to note that for cases 1 to 3, the enstrophy is lower than in the uncontrolled case, but the drag is higher. The drag reduction must therefore result from a different organization of the wake and not from its strength.

An inspection of the vorticity in the wake in Fig. **??**, the wakes corresponding to cases using the same porosity value, but different coating locations, are shown side-by-side, indeed

	Re = 550	
$\tau = 2.5\%d$	F_x	Enstrophy
case 0 (no control)	0.977	158.4
case 1	0.821 (-16%)	139.3 (-12%)
case 2	0.879 (-10%)	134.5 (-15%)
case 3	0.824 (-16%)	129.6 (-18%)
case 4	0.768 (-21%)	140.2 (-11%)
case 5	0.810 (-17%)	143.4 (-10%)

Table 4: Reduction effects brought by the different porous layer configurations in comparison to the uncontrolled case at Re=550 when $\tau = 2.5\%d$. From [2].

	Re = 3000	
$\tau = 2.5\%d$	F_x	Enstrophy
case 0 (no control)	0.926	334.2
case 1	1.011 (+9%)	318.4 (-5%)
case 2	1.018 (+10%)	283.7 (-15%)
case 3	0.929 (+0.4%)	271.1 (-19%)
case 4	0.806 (-13%)	331.4 (-0.8%)
case 5	0.828 (-10.5%)	320.6 (-4%)

Table 5: Same as Table **??** for $Re = 3000$. From [2].

shows that locating the porous coating at the tip of the semi-cylinder results in a narrower extent of the wake in the cross-stream direction, which explains why the resulting drag forces are less important in this configuration.

4. Conclusion We have shown two examples of wake control, illustrating the gain that can be obtained by adapting the control strategy to the geometry of the flow. The first example is a case of active flow control where tangential velocities are imparted on the flow. In this case we have shown that 3D profiles based on the natural 3D instabilities of the wake dramatically improve the control efficiency. In the second case we have shown that adjusting a porous layer around the separation points is more efficient than spreading the same layer with same porosity on the entire surface of the body.

Future plans are to combine the approached followed in these studies to optimize the location and width of the porous layer in more realistic 3D geometries of external mirrors.

These studies were done for low to intermediate Reynolds numbers (up to 1000 for the 3D case and 3000 for the 2D case). For higher Reynolds numbers, higher resolutions or LES simulation tools will be necessary to investigate control strategies. For higher Reynolds numbers, the friction drag dominates and one can also expect that different configurations and strategies will give more efficient control strategies.

Acknowledgment The authors acknowledge the support of the Agence National de la Recherche (ANR). Part of this research corresponds to a collaboration with Plastic Omnium and G.H. Cottet, Chlo Mimeau and Iraj Mortazavi thank Philippe Gilotte for fruitful discussions . G.-H. also acknowledges the support of Institut Universitaire de France (IUF).

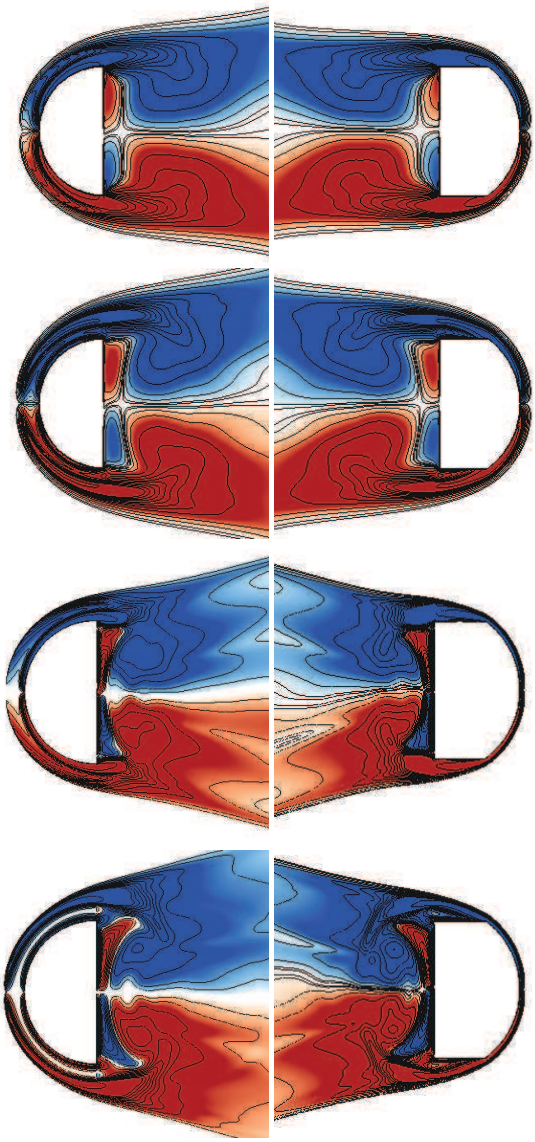

Figure 10: Vorticity in the near wake. Cases 4 and 5 are shown side-by-side with cases 1 and 3, repectively. From top to bottom : $Re = 550$, cases 1 and 4, $Re = 550$, cases 2 and 5, $Re = 3,000$, cases 1 and 4, $Re = 3,000$, cases 2 and 5. From [2].

References

[1] Poncet , P., Hildebrand R., Cottet, G.-H., and Koumoutsakos, P., Spatially distributed control for optimal drag reduction of the flow past a circular cylinder, *J. Fluid Mech.*, 599, 111-120, 2008.

[2] Mimeau, C., Mortazavi, I. and Cottet, G.-H., Passive flow control around a semi-circular cylinder using porous coatings, *International Journal of Flow Control*, special issue on Flow Control In Automotive Flows, to appear , 2014.

[3] Koumoutsakos, P., and Leonard, A., High-resolution simulations of the flow around an impulsively started cylinder using vortex methods'. *Journal of Fluid Mechanics*, 1995, pp. 1–38.

[4] Cottet, G.-H. and Poncet, P., Advances in direct numerical simulations of 3D wall-bounded flows by Vortex-in-Cell methods, *J. Comp. Phys.*, 193, 2004, 136-158.

[5] Cottet, G. H., and Koumoutsakos, P. D., *Vortex Methods - Theory and Practice*. Cambridge University Press, 2000.

[6] Coquerelle, M., and Cottet, G.-H., A vortex level set method for the two-way coupling of an incompressible fluid with colliding rigid bodies, *J. Comp. Phys.*, 227, 2008, 9121-9137.

[7] Tokumaru, P. & Dimotakis, P., Rotary oscillation of a cylinder wake, *J. Fluid Mech.*, 224 , 77–90, 1991.

[8] Dennis, S. C. R., Nguyen, P. & Kocabiyik, S., The flow induced by a rotationally oscillating and translating circular cylinder. *J. Fluid Mech.* 385, 255–286, 2000.

[9] Poncet, P., Topological aspects of the three-dimensional wake behind rotary oscillating circular cylinder. *J. Fluid Mech.*, 517, 27–53, 2004.

[10] Kim, J. and Choi, H., Distributed forcing of flow over a circular cylinder. *Phys. Fluids*, 17(3), 33-103, 2005.

[11] Milano, M., Koumoutsakos, P., A clustering genetic algorithm for cylinder drag optimization, *J. Comput. Phys.*, 175(1), 2002, 79-107.

[12] Koumoutsakos, P., Leonard, A., Pepin, F., Boundary Conditions for Viscous Vortex Methods, *J. Comput. Phys.*, 113, 1994, 52-61.

[13] Poncet, P., Analysis of direct three-dimensional parabolic panel methods. *SIAM J. Numer. Anal.*,, 2259-2297, 2007.

[14] Barkley, D. & Henderson, R. D., Three-dimensional Floquet stability analysis of the wake of a circular cylinder. *J. Fluid Mech.*, 322, 215–241, 1996.

[15] Bruneau, C. H., and Mortazavi, I., Numerical Modelling and Passive Flow Control Using Porous Media, *Computers & Fluids*, **37**, pp. 488–498, 2008.

[16] Angot, P., Bruneau, C. H., and Fabrie, P., A Penalization Method to Take Into Account Obstacles in Incompressible Viscous Flows, *Numerische Mathematik*, **81**, pp. 497–520, 1999.

[17] Hejlesen, M.M, Koumoutsakos, P., Leonard, A., Walther, J.H., *Iterative Brinkman penalization for remeshed vortex methods*, submitted, 2013.

[18] Gazzola, M., van Rees, W., and Koumoutsakos, P., C-start: optimal start of larval fish, *Journal of Fluid Mechanics, 698*, pp. 5–18, 2012.

[19] van Rees, W., Gazzola, M., and Koumoutsakos, P., Optimal shapes for anguilliform swimmers at intermediate reynolds numbers", *Journal of Fluid Mechanics, 722*, 2013.

[20] Beavers, G. D., and Joseph, D. D., Boundary Conditons at a Naturally Permeable Wall, *Journal of Fluid Mechanics, 30*, pp. 197–207, 1967.

[21] Breugem, W. P., Boersma, B. J., and Uittenbogaard, R. E., The Laminar Boundary Layer Over a Permeable Wall, *Transport in Porous Media, 59*, pp. 267–300, 2005.

[22] Hanspal, N. S., Waghode, A. N., Nassehi, V., and Wakeman, R. J., Numerical Analysis of Coupled Stokes/Darcy Flows in Industrial Filtrations, *Transport in Porous Media, 64*, pp. 73–101,2006.